
Causal Interpretable Progression Trajectory Analysis of Chronic Disease

Zhoujian Sun
 Zhejiang Lab
 sunzj@zhejianglab.com

Wenzhuo Zhang
 Zhejiang University
 zhangwenzhuo@zju.edu.cn

Zhengxing Huang
 Zhejiang University
 zhengxinghuang@zju.edu.cn

Nai Ding
 Zhejiang University
 ding_nai@zju.edu.cn

Abstract

Chronic disease is the leading cause of death, emphasizing the need for accurate prediction of disease progression trajectories and informed clinical decision-making. Machine learning (ML) models have shown promise in this domain by capturing non-linear patterns within patient features. However, existing ML-based models lack the ability to provide causal interpretable predictions and estimate treatment effects, limiting their decision-assisting perspective. In this study, we propose a novel model called causal trajectory prediction (CTP) to tackle the limitation. The CTP model combines trajectory prediction and causal discovery to enable accurate prediction of disease progression trajectories and uncovering causal relationships between features. By incorporating a causal graph into the prediction process, CTP ensures that ancestor features are not influenced by treatment on descendant features, thereby enhancing the interpretability of the model. By estimating the bounds of treatment effects, even in the presence of unmeasured confounders, the CTP provides valuable insights for clinical decision-making. We evaluate the performance of the CTP using simulated and real medical datasets. Experimental results demonstrate that our model achieves satisfactory performance, highlighting its potential to assist clinical decisions.

1 Introduction

Chronic disease (e.g., Alzheimer’s disease, heart failure) is the leading cause throughout the world [1]. Conducting prognosis studies tailored to the characteristics of chronic disease is widely regarded as an important way for assisting medical decision [2]. Previous studies usually evaluate patient prognosis by predicting the occurrence of an end-point event, e.g., death, significant decline of cognitive ability. A patient with high event occurrence probability will be identified as high-risk and requires extra attention. However, chronic disease affects many aspects of the patient’s body and defining a comprehensive end-point event is hard. To better handle this characteristic, recent research has begun utilizing long-term longitudinal data to predict trajectories of various patient features, rather than the occurrence of a single event [3, 4, 5]. In this process, machine learning (ML) models, particularly deep learning models, have shown superiority. These models may outperform

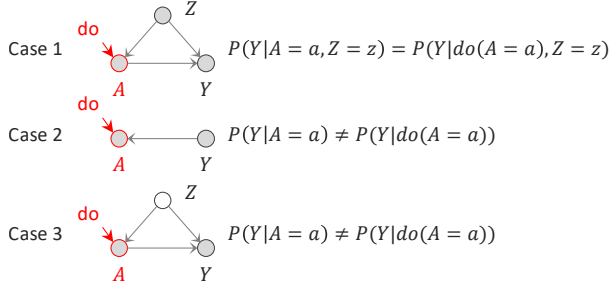


Figure 1: Causal Inference Assumptions. Most existing studies conduct treatment effect analysis in case one where A is the cause of Y and all confounders Z are observed. In practice, the cause structure is unknown and it is possible that A is the consequence of Y (case two) and there are unmeasured confounders (case three). Most existing studies cannot estimate treatment effect in case two and three. Gray circle indicates observed feature and white circle indicates unmeasured feature. “do” indicates treatment.

traditional linear models, such as logistic regression and Cox regression, in prediction performance, as they are better at fitting non-linear patterns within patient features.

Despite achieving impressive predictive performance, ML-based models still face challenges in assisting medical decisions due to the lack of causal interpretability [6]. Chronic disease has complex, heterogeneous, and sometimes unknown etiologies. A model that only predicts a patient’s poor prognosis, no matter how accurate, doesn’t enable clinicians to provide targeted treatments to improve the prognosis. What clinicians require are causal interpretable models. These models can not only predict future trajectories accurately but can also answer counterfactual inquiries such as “What changes will occur in the trajectory of a interested feature if we change the value of a treatment feature from a to b?” (i.e., treatment effect prediction) [7]. Clinical decision-making is feasible when the model can help clinicians anticipate the consequences of their actions. Unfortunately, most ML-based models cannot answer such inquiries, as they only capture correlational relationships between features [6].

To tackle this limitation, many studies have proposed models to estimate medical treatment effects using observational datasets [8]. However, these models often adopt two strong assumptions which may not hold in reality (Figure 1). The first assumption is that the treatment feature A is the cause of a interested feature Y (i.e., $A \rightarrow Y$). In practice, we do not always know the causal structure in advance and it is possible that A is actually a consequence of Y (i.e., $A \leftarrow Y$). If A is a consequence of Y , a change in A will not affect Y , and existing causal inference models may generate incorrect prediction due to they capture correlation relationship between two features [9]. The second assumption is that there are no unmeasured confounders (i.e., strong ignorability). As the development mechanisms of many chronic diseases are unclear, there may exist unmeasured confounders that we do not realize. Therefore, these models may generate unreliable estimations due to confounding bias[10, 11].

This study aims to propose a new framework without these two assumptions to achieve causally interpretable disease progression trajectory analysis. Intuitively, the framework needs to discover the causal structure between features and ensure the trajectory of every feature is predicted only by itself and its causative features. Then, we can generate an unaffected trajectory of Y under treatment A when A is a descendant of Y . In this study, we treat interested features Y include all observable features. The framework also needs to infer the effect of unmeasured confounders, so the treatment effect can be appropriately estimated. It’s important to note that the effect of an unmeasured confounder may be unidentifiable as there are infinite models that can generate the observed dataset when an unmeasured confounder exists [12, 13, 14]. Therefore, we only aim to estimate the possible bounds of the treatment effect when unmeasured confounder exists, rather than implementing point-estimation of the treatment effect.

We designed a framework consisting of two phases to achieve our goal. The first phase uses a causal trajectory prediction (CTP) model to predict disease progression trajectory in a causal manner. This model formulates the disease trajectory prediction problem as solving ordinary differential equations (ODE). It estimates features’ derivatives using neural networks, and trajectories can be predicted via

a numerical neural ODE solver [15]. The CTP model also adopts a *neural connectivity matrix* to evaluate the predictive effect with respect to each feature pair [16]. To ensure each feature is predicted only by itself and its causative features, we applied a sparse penalty and a score based penalty to the neural connectivity matrix. Previous studies have demonstrated that it is possible to discover causal structures in a linear dynamical system using penalties [14, 17, 18]. In this study, we extend this approach to a non-linear system. Once the CTP model is optimized and the causal structure is identified, we train a group of new CTP models to estimate the bounds of the treatment effect (the second phase). The training goal is that the group of new CTP models need to fit the observed dataset accurately and generate trajectories as different as possible when we apply a treatment. Finally, we estimate the treatment effect bounds by analyzing trajectories generated by the group of optimized new CTP models.

We investigate the performance of the framework in discovering causal relationships between features, predicting disease progression trajectories, and predicting treatment effects. We utilize one real longitudinal medical datasets and four simulated datasets to evaluate model performance. Experiment results indicate that our framework is able to reconstruct the causal graph within features, obtain satisfactory predictive performance, and evaluate the bound of treatment effects well. Therefore, we believe the framework introduces a new way to assist clinical decisions.

2 Related Work

2.1 Trajectory Prediction

Recurrent neural network (RNN) and Transformer are widely used to learn representations from sequential patient data and predict their disease progression trajectories [19, 20]. However, these two types of methods are designed to model discrete trajectory with fixed time interval, while we may need to generate continuous patient trajectory. Recent studies usually adopted two kinds of methods to model continuous trajectories. The first method is to model the trajectory prediction problem as solving a dynamical system. Benefit from the neural ODE solver [15], it is possible to optimize a neural network parameterized dynamical system, so that predicting continuous patient trajectory is feasible. For example, Seedat et al. interprets the data as samples from an underlying continuous time process and models its latent trajectory explicitly using controlled differential equations [21]. Alaa et al. temporally integrate embeddings of clinical codes and neural ODEs to learn and predict patient trajectories in electronic health records [22]. The second method models continuous trajectories by revising the architecture of the RNN or transformer. For example, Duan et al. utilize the Hawkes process to learn the effect of time interval and incorporate Hawkes process into a RNN model [23]. Tan et al. propose an end-to-end model that preserves the informative varying intervals by introducing a time-aware structure to directly adjust the influence of the previous status in coordination with the elapsed time [24]. Besides, Tipirneni et al. regard the irregularity as data missing and overcome the pitfall by treating time-series as a set of observation triplets instead of using the standard dense matrix representation [25].

Although these models claimed they obtained impressive performance, they usually cannot be applied to treatment effect analysis due to they did not capture causal information within data.

2.2 Causal Discovery

As far as we know, there are generally two kinds of methods can discover causalities from sequential data. The first is to use a ODE based linear dynamic system to model the data generating process and adopt a sparse penalty (e.g., ridge loss) to eliminate unnecessary feature interactions. Previous studies have proved this approach can reconstruct causal structure correctly given observational data [26]. Known as physics informed network (PIN), this method is widely used to discover govern equations in physical processes [17, 18]. The second method utilize the Granger causality assumption that assume each sampled variable is affected only by earlier observations. Then they summarize the causal graph by analyzing the Granger causality information. For example, Cheng et al use a threshold-based method to reserve probable Granger causality between features [27]. Amornbunchornvej et al. propose a regression and sparse based algorithm to identify Granger causality from data [28]. In this study, we adopt the first framework to discover causal graph in a non-linear dynamic system.

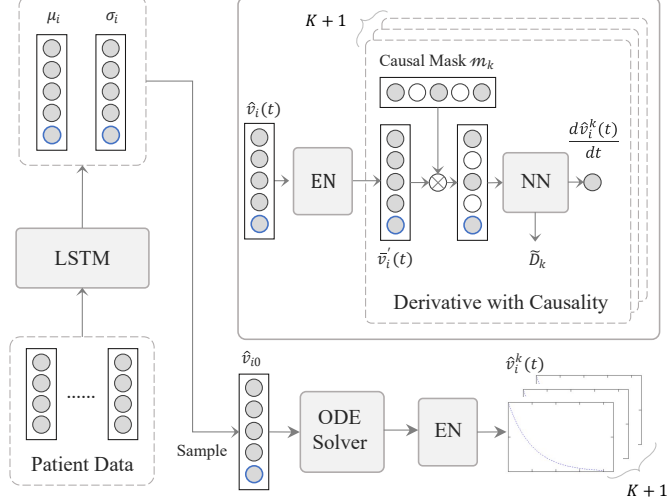


Figure 2: Causal Trajectory Prediction (CTP) Model

2.3 Treatment Effect Estimation with Hidden Confounder

Most previous studies tried to infer the value or the posterior distribution of hidden confounder given the observed data. Once the value or the distribution of confounder is inferred, the treatment effect can be evaluated by adjusting. For example, Bica et al. use a RNN with multitask output to infer unmeasured confounders that render the assigned treatments conditionally independent [29]. Similarly, Ma et al. aim to learn how hidden confounders behave over time by using observation data and historical information. [30]. Cao et al. leverage Lipschitz regularization and neural controlled differential equations to capture the dynamics of hidden confounders [31]. Ashman et al. develop a gradient and generative based model to infer the existence and effect of hidden confounders simultaneously [32]. Wang et al. propose a clipping strategy to the inverse propensity score estimation to reduce the variance of the learning objective [33].

Although these studies obtained impressive progress, they did not discuss whether the effect of unmeasured confounder is identifiable. In fact, the effect unmeasured confounder is generally unidentifiable for both static dataset and sequential datasets [12, 13, 14]. Therefore, we argue it may be too optimistic to presume deconfounding is feasible and only try to estimate the bound of the treatment effect when confounder exists [10].

3 Method

3.1 Preliminary

We denote a dataset consists of a sequence of a two-element tuple $(s_i, l_i)_{i=1}^N$, $s_i = (v_{ij}, m_{ij}, t_{ij})_{j=1}^{N_i^s}$ indicates a sequence of patient visit data until time point $t_{iN_i^s}$, and N_i^s means the number of visits. v_i denotes progression trajectory of the i -th patient, and $v_i(t)$ is a vector with K elements that denotes patient characteristics at timepoint t . v_{ij} means data in the j -th visit (or it can be regarded as the abbreviation of $v_i(t_{ij})$), and v_{ij}^k denotes the value of the k -th feature. $v_{ij}^k(t)$ can be a continuous variable or a discrete variable. In this study, we presume discrete variables are binary for simplicity, while the proposed method can be generalized to handle categorical variables naturally. $m_{ij} \in \{0, 1\}^K$ indicates whether a corresponding feature in v_{ij} is missing (1 indicates missing). $l_i = (v_{ij}, m_{ij}, t_{ij})_{j=N_i^s+1}^{N_i^s+N_i^l}$ indicates a sequence of (label) data need to be predicted.

We use a numerical adjacency matrix to describe the causal structure between features $D \in \mathbb{R}_{\geq 0}^{(K+1) \times (K+1)}$ [34]. $D_{kl} = 0$ indicates the k -th feature is not the cause of the l -th feature, and $D_{kl} \neq 0$ means k -th feature is a cause of the l -th feature. Without loss of generality, D uses an extra dimension to describe the causal relationship between observed features and an unmeasured

confounder [35]. In this study, we presume the progression of the unmeasured confounder is not the consequence of any observed features.

3.2 Causal Trajectory Prediction

3.2.1 Trajectory Prediction

We estimate patient disease progression trajectory $\hat{v}_i(t)$ by solving ODEs (Figure 2) [15]. Our CTP model first estimates the value of patient characteristics $\hat{v}_{i0} \in \mathbb{R}^{K+1}$ at an initial time point t_0 . We follow a standard variational autoencoder to estimate the posterior of the $q(\hat{v}_{i0}|s_i)$, where $q(\hat{v}_{i0}|s_i)$ follows a Gaussian distribution with a diagonal covariance matrix, t_0 is a custom number. We use a long-short term memory (LSTM) network parameterized by ϕ to estimate μ_i, σ_i (Equation 1). Then, we randomly sample the \hat{v}_{i0} via the reparameterization trick (Equation 2) [36]. Our CTP model estimates the change rate of \hat{v}_i (Equation 3). The $\hat{v}_i(t)$ can be estimated according to f_θ and v_{i0} via a differential numerical ODE solver (Equation 4) [15]. As ODE based models is only capable of modeling the dynamics of continuous variables, the \hat{v}_i^k in fact represents logit values, rather than the true value, for discrete variables.

$$[\mu_i, \sigma_i] = \text{LSTM}([v_{ij}, m_{ij}, t_{ij}]_{j=1}^{N_i^s}; \phi). \quad (1)$$

$$q(\hat{v}_{i0}|s_i) = \mathcal{N}(\hat{v}_{i0}|\mu_i, \sigma_i). \quad (2)$$

$$\frac{d\hat{v}_i(t)}{dt} = f_\theta(\hat{v}_i(t)). \quad (3)$$

$$\hat{v}_i(t) = \text{ODESolver}(f_\theta, \hat{v}_{i0}, t_0, t). \quad (4)$$

3.2.2 Derivative with Causality

We carefully design the f_θ to ensure the CTP model predict feature trajectory in a causal interpretable manner. We first mapping the $\hat{v}_i^k(t)$ to $\bar{v}_i^k(t)$ (Equation 5), which is an identical mapping for continuous variables and discretizes logit for discrete variables [37].

$$\bar{v}_i^k(t) = \begin{cases} \hat{v}_i^k(t), & \text{continuous variable} \\ \text{Gumbel_Sigmoid}(\hat{v}_i^k(t)), & \text{discrete variable} \end{cases} \quad (5)$$

Then, we use $K+1$ independent components f_{θ_k} to predict each $\frac{d\hat{v}_i^k(t)}{dt}$ (Equation 6), where \circ means element-wise multiplication. \mathcal{M}_k is a causal mask which will be introduced later and it can be regarded as a vector whose all elements are one at present.

$$\frac{d\hat{v}_i^k(t)}{dt} = f_{\theta_k}(\bar{v}_i(t) \circ \mathcal{M}_k). \quad (6)$$

The core of causal interpretability is to ensure a feature is predicted only by itself and its cause features. Here, we introduce the **neural network connectivity** to evaluate predict effect of a feature [16]. Specifically, the form of a feed-forward neural network (without bias term, the output is a real number) follows:

$$o = W_N \sigma(\cdots \sigma(W_2(\sigma(W_1 x)))), \quad (7)$$

where $x \in \mathbb{R}^{K+1}$ is the input, $o \in \mathbb{R}$ is the output, σ is the non-linear activation, and W_1, \dots, W_N is a series of weight matrices (vectors). The connectivity vector $C \in \mathbb{R}^{K+1}$ follows:

$$C = |W_N| \cdots |W_2| |W_1|. \quad (8)$$

It is easy to find that $C_j = 0$ indicates the j -th element does not affect the output. Based on the fact, we can derive \tilde{D} (Equation 9).

$$\tilde{D}_{jk} = C_j^k, \quad (9)$$

where C^k are the connectivity vector for f_{θ_k} . \tilde{D} analogs an adjacent matrix where a non-zero elements \tilde{D}_{jk} represents the j -th feature can predict the k -th feature somehow. We can use sparse penalty to \tilde{D} to remove spurious causal connections 10) [17].

$$g(\theta) = \sum_{i=1}^{K+1} \sum_{j=1}^{K+1} (\tilde{D})_{ij}. \quad (10)$$

Moreover, the causal relationship between features can be characterized as a DAG in many disease [38, 39]. For example, the causal relation of features in amyloid beta pathway in Alzheimer's disease formulates a DAG [40]. In this study, we additionally presume the causal graph is a DAG and applied an extra score based penalty to \tilde{D} in this study (Equation 11, [41]).

$$h(\theta) = \text{Tr}(\exp((1 - I) \circ \tilde{D})) - K, \quad (11)$$

where Tr means the trace of a matrix, and $\exp(A)$ denotes the exponential of a non-negative square adjacent matrix A that is defined as the infinite Taylor series, i.e., $\exp(A) = \sum_{k=0}^{\infty} \frac{1}{k!} A^k$, $A^0 = I$. $(1 - I) \circ \tilde{D}$ formulates a DAG if and only if $h(\theta) = 0$. We use $(1 - I)$ to denote we allow self-loop (i.e., a feature is predictive to its derivative). Previous studies proofed A_{ij}^k means a weighted path count from element i to j after k step, and the count is a non-negative number. Therefore, if the A represents a cyclic graph, there must be some $A_{ii}^k > 0$, and cause $\text{Tr}(\exp(A)) - K > 0$. The DAG constraint equals zero if and only if the A represents a DAG. Once the constrained hold, it is possible that every $v_i^k(t)$ is predicted only by itself, and its cause features, and so that the model is causal interpretable.

3.2.3 Optimization

We optimize parameters by minimizing the \mathcal{L} (Equation 12). The optimizing goal is perfectly reconstructing observed data when j is less or equal than N_i^s , and accurately predicting future trajectory when j is greater than N_i^s . The mean square error (MSE) is used to measure the difference in continuous variables, and cross entropy (CE) is used for discrete variables. B is a mini batch of dataset and $|B|$ indicates its size.

$$\mathcal{L} = \sum_{i,j,k}^{|B|, N_i^s + N_i^l, K} \begin{cases} \text{MSE}(v_{ij}^k, \hat{v}_{ij}^k), & v_{ij}^k \text{ is continuous} \\ \text{CE}(v_{ij}^k, \hat{v}_{ij}^k), & v_{ij}^k \text{ is discrete} \\ 0, & v_{ij}^k \text{ is missing} \end{cases}. \quad (12)$$

Finally, the objective function of this study follows Equation 13. One can also add extra L1-regularization to \tilde{D} to ensure the sparsity of the graph if needed.

$$\min_{\theta, \phi} (\mathcal{L} + \beta g(\theta)) \quad \text{s.t. } h(\theta) = 0, \quad (13)$$

where β is the weight of sparse penalty. Augmented Lagrangian method can optimize parameters by optimizing a sequence of unconstrained subproblems (Equation 14) [16, 41]. In our study, each subproblems is:

$$\mathcal{L}_{final} = \mathcal{L} + \beta g(\theta) + \frac{\rho}{2} h(\theta)^2 + \alpha h(\theta), \quad (14)$$

where ρ, α are penalty weights, respectively. We approximately solve each subproblem via stochastic gradient descent method. The details of optimization process are described in Algorithm 1. The line 2 to 19 describes the details of generating Lagrangian multiplier, while line 20 to line 24 describes a normal gradient based parameters optimization process. During the optimization process, we calculate

Algorithm 1 CTP Model Optimize Process

Input: training data D_t , validation data D_v , max iteration n , update interval m , convergence threshold δ , Lagrangian parameters $\alpha, \rho, \eta, \gamma$

Output: Loss \mathcal{L} , parameters ϕ, θ

Initialize : ϕ, θ , loss list $a_1: []$, $a_2: []$

1: **for** $i = 1$ to n **do**

2: **if** $i \bmod m = 0$ **then**

3: Calculate \mathcal{L}_{final} according Equation 14 given D_v

4: Calculate $h(\theta)$ according to Equation 11

5: Append \mathcal{L}_{final} to loss list a_1

6: Append $h(\theta)$ to loss list a_2

7: **end if**

8: **if** $(i \bmod m) == 0$ and $i > 2m$ **then**

9: **if** $a_1[-1] < a_1[-2]$ **then**

10: $\Delta\lambda = (a_1[-2] - a_1[-1])/m$

11: **if** $\Delta\lambda < \delta$ **then**

12: $h = a_2[-1]$

13: $\rho = \alpha h + \rho$

14: **if** $a_2[-1] > a_2[-2] \times \gamma$ **then**

15: $\alpha = \eta \times \alpha$

16: **end if**

17: **end if**

18: **end if**

19: **end if**

20: Sample mini-batch B from D_t

21: Calculate \mathcal{L}_{final} according Equation 14 given B

22: Calculate gradient $\nabla \mathcal{L}_{final}$ w.r.t. ϕ, θ

23: Update ϕ, θ via a stochastic optimizer

24: **end for**

25: Calculate \mathcal{L} according Equation 12 given D_v

26: **return** $\mathcal{L}, \phi, \theta$

and record \mathcal{L}_{final} and $h(\theta)$ every m steps (line 3-7). We regard a subproblem is solved when it converges (line 9-11). Then, we gradually increase the value of α and ρ (line 13-15) and establish a new subproblem. Eventually, all connections violate the DAG assumption between features will to be eliminated.

The back-propagation method requires to compute the gradient of all parameters, while numerical ODE solver is typically undifferentiable. In this study, we adopted the adjoint sensitive method to make ODE solver differentiable and backpropagation method feasible [15].

3.2.4 Causal Graph Identification

Our CTP model still faces challenges in discovering causal relationship between features. The first challenge is that the value of \tilde{D}_{ij} is basically cannot be penalized to exactly zero, but a very small number, as we use a numerical optimizer. The model is also fragile because the neural ODE and matrix exponential operation in the CTP model is sensitive to parameter initialization and input noise [42]. The CTP model is easy to converge to a bad point when the initial parameter is not good. Even the CTP model converges to a satisfactory point and obtains good prediction performance, it is easy to identify causal edges with wrong causal direction. We adopted the Algorithm 2 to tackle above limitations. The algorithm uses the $\mathcal{M} \in \{0, 1\}^{(K+1) \times (K+1)}$ to describe causal relation between features and $\tilde{\mathcal{M}} \in \{0, 1\}^{(K+1) \times (K+1)}$ to determine whether the causal relationship is certain. We use the Equation 15 to initialize \mathcal{M} and $\tilde{\mathcal{M}}$, where \mathcal{M}_{ij} indicates i -th feature is the cause of the j -th feature, and $\tilde{\mathcal{M}}_{ij} = 1$ indicates the \mathcal{M}_{ij} is not certain. At the beginning, every causal relation is uncertain. Of note, we set $\mathcal{M}_{ij} = 0$ when $i = K + 1$ and $j \leq K$ because we presume the hidden confounder is not the consequence of observed features. We define all valid causal connection is uncertain at start.

Algorithm 2 Causal Identification

Input: training data D_t , validation data D_v , accept ratio ρ , model threshold δ , causal threshold φ , model number N ,
Output: Causal Mask \mathcal{M}

Initialize : $\mathcal{M} \leftarrow \widetilde{\mathcal{M}}$ via Eq. 15

```

1: while  $\sum_{ij}(\widetilde{\mathcal{M}}_{ij}) > 0$  do
2:   Define model list M_List = []
3:   while Length(M_List) <  $N$  do
4:     Optimize a new model via Alg. 1, obtain  $\mathcal{L}, \phi, \theta$ 
5:     Summarize  $\widetilde{D}$  according  $\theta$  via Eq. 9
6:     if  $\mathcal{L} < \delta$  then
7:       Append  $\widetilde{D}$  to M_List
8:     end if
9:   end while
10:  for  $i = 1, j = 1$  to  $K + 1, K + 1$  do
11:    for  $n = 1$  to  $N$  do
12:       $e_{ij} = 0$ 
13:      if  $M_{List[n]}_{ij} < \varphi$  then
14:         $e_{ij} = e_{ij} + 1$ 
15:      end if
16:    end for
17:    if  $\widetilde{\mathcal{M}}_{ij}$  and  $e_{ij}/N > \rho$  then
18:       $\mathcal{M}_{ij} = 0$ 
19:       $\widetilde{\mathcal{M}}_{ij} = 0$ 
20:    else if  $\widetilde{\mathcal{M}}_{ij}$  and  $e_{ij}/N < (1 - \rho)$  then
21:       $\mathcal{M}_{ij} = 1$ 
22:       $\widetilde{\mathcal{M}}_{ij} = 0$ 
23:    end if
24:  end for
25: end while
26: return  $\mathcal{M}$ 

```

$$\mathcal{M}_{ij}, \widetilde{\mathcal{M}}_{ij} = \begin{cases} 1, & j \leq K \\ 0, & j = K + 1 \text{ and } i \leq K \\ 1, & j = K + 1 \text{ and } i = K + 1 \end{cases} . \quad (15)$$

The algorithm first repeatedly optimize independent CTP models and records N models that can converge successfully (i.e., validation loss \mathcal{L} is less than a predefined threshold δ) (line 2-8). We presume these models are more probable to identify correct causal relationships. Then, We analyzes the neural connectivity matrix of each model. We treat elements whose value is less than a threshold φ as invalid (line 12) [16]. We use the e_{ij}/N to determine how many models treat the connection $i \rightarrow j$ as invalid. If the value is larger than an accept ratio ρ , we will treat the connection as certainly invalid and set $\mathcal{M}_{ij} = 0$ and $\widetilde{\mathcal{M}}_{ij} = 0$. e_{ij}/N is less than $1 - \rho$ indicates the connection is certainly valid and we set $\mathcal{M}_{ij} = 1$ and $\widetilde{\mathcal{M}}_{ij} = 0$ (line 16-21). We repeat run the process until all causal relations become certain (i.e., $\sum_{ij}(\widetilde{\mathcal{M}}_{ij}) = 0$))

3.3 Treatment Effect Analysis

We conduct treatment effect analysis under two assumptions. (1) the CTP model optimized in the last subsection (denoted as M^*) predicts the disease progression trajectory accurately. (2) The M^* summarizes reliable causal structure between observed features and the unmeasured confounder. However, it is challenging to evaluate the effect of a treatment when unmeasured confounder exists because parameters in the M^* is not the only solution to for the prediction problem. There are infinite choice of other parameters also generate the observed data when unmeasured confounder exists [43].

Algorithm 3 New CTP Models Optimize Process

Input: $D_t, L, M^*, \text{lr}_p, \text{lr}_t, \text{optim}_p, \text{optim}_t$
Output: A series of new CTP model $\{M_l\}_{l=1}^L$

Initialize : Parameters of $\{M^l\}_{l=1}^L$ via M^*

- 1: **for** $j = 1$ to n **do**
- 2: Sample mini-batch B from D_t
- 3: Define prediction loss $\mathcal{L}_p = 0$
- 4: **for** $l = 1$ to L **do**
- 5: Calculate \mathcal{L}_l via Eq. 12 given B and M_l
- 6: $\mathcal{L}_p = \mathcal{L}_p + \mathcal{L}_l$
- 7: **end for**
- 8: Define treatment loss $\mathcal{L}_{treat} = 0$
- 9: Define estimation list $\text{EL} = []$
- 10: Randomly sample $t_a > t_0$ and $t_o > t_a$
- 11: **for** $l = 1$ to L **do**
- 12: Apply treatment $\text{do}(A^{t_a} = a)$ to M_l
- 13: **for** $i = 1$ to $|B|$ **do**
- 14: Calculate ${}^l\hat{v}_i$ via Eq. 4 given M^l and s_i from B
- 15: Append ${}^l\hat{v}_i(t_o)$ to EL
- 16: **end for**
- 17: **end for**
- 18: Compute pairwise distance \mathcal{L}_t of EL via Eq. 16
- 19: Calculate gradient $\nabla \mathcal{L}_p$, and $\nabla \mathcal{L}_t$
- 20: Minimize \mathcal{L}_p via $\nabla \mathcal{L}_p$, optim_p , and lr_p
- 21: Maximize \mathcal{L}_t via $\nabla \mathcal{L}_t$, optim_t , and lr_t
- 22: **end for**
- 23: **return** $\{M^l\}_{l=1}^L$

These choices of parameters generate different trajectories under a treatment. In this study, we further presume all feasible parameters are located in a region.

As we lack the ability to identify which choice of parameters is better, this study only aims to estimate the probable bound of the trajectory under a treatment. We adopt a intuitive idea that trains a series of new CTP models that cover the parameters region (Algorithm 3). New CTP models share the same structure according to the M^* and inherit its causal mask \mathcal{M} and parameters. We only optimize the reconstruct loss and prediction loss during training (line 4-6, Equation 12).

We use $\text{do}(A^{t_a} = a)$ to denote a treatment, which means fix the value of feature A to a from a time point t_a (line 12), regardless its original value. Given a patient data s_i (from B) and a model M^l , we can implement treatment effect analysis by performing $\text{do}(A^{t_a} = a)$. Then, we use a ODE solver to solve the ODEs, and the solver will generate disease progression trajectory ${}^l\hat{v}_i(t)$ under a treatment (line 14). Of note, M^l evaluates treatment effect appropriately. By utilizing the causal mask \mathcal{M} from M^* , we can access the causal relationship between features and ensure the dynamics of ancestral features of A will not be affected. Meanwhile, M^l infers the value of unmeasured confounder so that we can adjust confounding bias. We record the patient characteristics ${}^l\hat{v}_i(t_o)$ at a randomly selected time point t_o (line 15). To make trajectories of M^l as dissimilar as possible, we maximize the pair-wise distance between recorded ${}^l\hat{v}_i(t_o)$ (Equation 16). In this study, we applied the simplest p-norm distance for computational efficiency. However, more sophisticated loss function such as Wasserstein distance is also applicable [10].

$$\mathcal{L}_t = \sum_{i=1}^{|B|} \sum_{j=1}^{L-1} \sum_{k=i+1}^L \text{Distance}({}^j\hat{v}_i(t_o), {}^k\hat{v}_i(t_o)), \quad (16)$$

The optimization problem is actually a min-max problem which minimize the prediction loss \mathcal{L}_p and maximize the treatment \mathcal{L}_t . We use two gradient-based optimizers to update parameters alternatively, which is widely used in similar studies (line 18-21) [44].

	Hao	Zheng	MM-25	MM-50	ADNI
# of Samples	1,024	1,024	1,024	1,024	275
Avg. Visit	15	15	15	15	3.7
# Features	4	4	20	45	88
Avg. Interval	1.00	2.00	0.25	0.25	1.65
Continuous	Yes	Yes	Yes	Yes	No

Table 1: Dataset Statistics

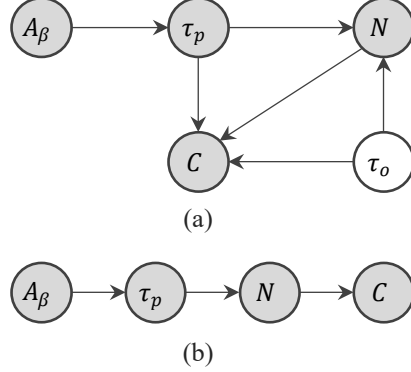


Figure 3: Causal Graph of Simulated Data. (a) Hao model. (b) Zheng model. The causal graph only describes causal relation between different features.

Once the series of new CTP models are optimized, we can obtain the maximum/minimum possible value of a feature i at time point t across L candidates via Equation 17, and then summarize the trajectory bound.

$$\max({}^l\hat{v}_i(t))/\min({}^l\hat{v}_i(t)), \quad (17)$$

4 Experiment

4.1 Dataset and Preprocessing

We used four simulated datasets and one real medical dataset to conduct experiment, whose statistics is in Table 1.

4.1.1 Amyloid Beta Pathway Simulated Dataset

We used the amyloid beta pathway, an extensively investigated disease progression pathway of the Alzheimer's disease, to conduct analysis [40, 45, 1, 46]. We used two recently published ODE based bio-mathematical model to instantiate the pathway.

Hao model [40]. This model includes five features, i.e., amyloid beta (A_β), phosphorylated tau protein (τ_p), nonamyloid-dependent tauopathy (τ_o), neurodegeneration (N), and cognitive decline score (C). It describes the dynamics of the pathway on three different groups of patients, i.e., Alzheimer's disease, late mild cognitive impairment (LMCI), and cognitive normal groups. The dynamics of three groups shares the same form of ODEs but with different parameters (Equation 18). In this study, we chose the group of parameters and initial conditions of LMCI generate simulated dataset. The initial time t_0 is 50, and the parameters of the system follows: $A_0 = 41.57$, $\tau_{p0} = 4.21$, $\tau_{o0} = 28.66$, $N_0 = 0.48$, $C_0 = 6.03$, $\lambda_{A_\beta} = 0.1612$, $K_{A_\beta} = 264.99$, $\lambda_\tau = 0.08$, $K_{\tau_p} = 131.66$, $\lambda_{\tau_o} = 1.74$, $\lambda_{N_{\tau_p}} = 0.000424$, $\lambda_{N_{\tau_o}} = 0.00737$, $K_N = 1.02$, $\lambda_{CN} = 1.26$, $\lambda_{C_\tau} = 1.93$, $K_C = 129.4$. We chose LMCI because it is a risk state that leads the real Alzheimer's disease. The oracle causal relationship between features is shown in Figure 3(a) [40]. Compared to the original setting of Hao model, we add an extra link between τ_o and C to introduce confounder structure but does not

re-estimate the parameters [46]. We discard τ_o during experiment process to introduce unmeasured confounder. Therefore, the dataset has four observable features.

$$\left\{ \begin{array}{l} \frac{dA_\beta}{dt} = \lambda_{A_\beta} A_\beta \left(1 - \frac{A_\beta}{K_{A_\beta}}\right) \\ \frac{d\tau_p}{dt} = \lambda_\tau A_\beta \left(1 - \frac{\tau_p}{K_{\tau_p}}\right) \\ \frac{d\tau_o}{dt} = \lambda_{\tau_o} \\ \frac{dN}{dt} = (\lambda_{N_{\tau_o}} \tau_o + \lambda_{N_{\tau_p}} \tau_p) \left(1 - \frac{N}{K_N}\right) \\ \frac{dC}{dt} = (\lambda_{CN} N + \lambda_{C\tau} (\tau_p + \tau_o)) \left(1 - \frac{C}{K_C}\right) \end{array} \right. . \quad (18)$$

Zheng Model [45]. This model includes four features (i.e., A_β , tau protein τ , N , and C) with the causal structure shown in Figure 3(b). Zheng model does not contain unmeasured features and all four features are observable. Zheng model describes the dynamics of LMCI and Alzheimer's disease and its form follows Equation 19. The initial DPS time t_0 is -10, $A_\beta(t_0) = y_0$, $\tau_p(t_0) = 0$, $\tau_o(t_0) = 0$, $N(t_0) = 0$, and $C(t_0) = 0$ and the parameters follows: $w_{A0} = 0$, $w_{A1} = 0.745$, $w_{A2} = -0.749$, $w_{\tau0} = 0$, $w_{\tau1} = 0.689$, $w_{\tau2} = -0.679$, $w_{\tau3} = 0$, $w_{\tau4} = 0.185$, $w_{\tau5} = -0.101$, $w_{\tau6} = 0$, $w_{N0} = 0$, $w_{N1} = 0.899$, $w_{N2} = -0.927$, $w_{N3} = 0.554$, $w_{N4} = 1.792$, $w_{N5} = -2.127$, $w_{C0} = 0$, $w_{C1} = 0.134$, $w_{C2} = -0.067$, $w_{C3} = 0.004$, $w_{C4} = 0.007$, $w_{C5} = -0.008$, $y_0 = 0.000141$.

$$\left\{ \begin{array}{l} \frac{dA_\beta}{dt} = w_{A1} A_\beta + w_{A2} A_\beta^2 \\ \frac{d\tau}{dt} = w_{\tau1} \tau + w_{\tau2} \tau^2 + w_{\tau3} A_\beta + w_{\tau4} A_\beta^2 + w_{\tau5} A_\beta \tau \\ \frac{dN}{dt} = w_{N1} N + w_{N2} N^2 + w_{N3} \tau + w_{N4} \tau^2 + w_{N5} \tau N \\ \frac{dC}{dt} = w_{C1} C + w_{C2} C^2 + w_{C3} N + w_{C4} N^2 + w_{C5} NC \end{array} \right. . \quad (19)$$

For each model, we generated training, validation, and test datasets with 1,024, 128, 128 samples, respectively [47]. Each sample contains 15 observations distributed evenly. We added Gaussian noise to the initial value and each feature observation. We randomly discard 5% observations to simulate missing data. We define observations before the eighth observation is used as the input and reconstruction target of the CTP, and observations after eighth observation is only used for prediction. We normalized all variables to a zero mean unit variance distribution after data generating process.

4.1.2 MK Dataset

We also generated two Michaelis-Menten kinetics datasets (i.e., MM-25, MM-50) to evaluate the performance of the CTP model in high-dimensional case [48]. The original MM-25 contains 25 nodes and the original MM-50 contains 50 nodes. The causal relation and dynamics of two datasets follows Equation 20, where X_i denotes a node and N_i denotes the set of the parent nodes of X_i . The causal relation was from a randomly generated DAG whose edge probability was 0.15, and the vertices follows the topological order. The initial value of each node is a sample of a uniform distribution that takes value between 0.8 and 1.2. The initial time is zero. Each sequence contains uniformly distributed 15 visits and time interval was 0.25. We randomly discarded 5% observations to introduce missing dataset and did not add observational noise. For each model, we generated training, validation, and test datasets with 1,024, 128, 128 samples, respectively. Finally, we discarded the first five node to introduce unmeasured confounding. The final MM-25 and MM-50 dataset contains 20 and 45 features, respectively.

$$\frac{dX_i}{dt} = -X_i + \frac{1}{|N_i|} \sum_{j \in N_i} \frac{X_j}{1 + X_j}. \quad (20)$$

Model	Dataset	Combined		Reconstruct		Predict	
		Loss	AUC	RMSE	AUC	RMSE	AUC
Linear ODE	ADNI	0.29±0.03	0.58±0.02	0.26±0.02	0.67±0.02	0.26±0.02	0.46±0.02
Neural ODE	ADNI	0.30±0.01	0.62±0.02	0.22±0.01	0.69±0.01	0.45±0.03	0.54±0.02
NGM	ADNI	0.27±0.02	0.59±0.01	0.23±0.02	0.68±0.01	0.34±0.02	0.53±0.01
TE-CDE	ADNI	0.25±0.02	0.61±0.01	0.24±0.01	0.66±0.01	0.30±0.01	0.52±0.01
CF-ODE	ADNI	0.27±0.01	0.60±0.01	0.21±0.03	0.69±0.02	0.32±0.03	0.54±0.01
CTP	ADNI	0.24±0.01	0.65±0.01	0.20±0.01	0.73±0.01	0.29±0.02	0.55±0.02

Table 2: ADNI Data Prediction Performance

Model	Dataset	Combined		Reconstruct		Predict	
		Loss	AUC	RMSE	AUC	RMSE	AUC
Linear ODE	Hao	0.29±0.03	0.05±0.01	0.12±0.03			
Neural ODE	Hao	0.02±0.01	0.01±0.00	0.01±0.00			
NGM	Hao	0.04±0.01	0.02±0.01	0.02±0.01			
TE-CDE	Hao	0.03±0.01	0.02±0.01	0.01±0.00			
CF-ODE	Hao	0.03±0.01	0.02±0.00	0.01±0.00			
CTP	Hao	0.03±0.02	0.01±0.01	0.02±0.00			
Linear ODE	Zheng	0.32±0.05	0.17±0.03	0.15±0.02			
Neural ODE	Zheng	0.17±0.02	0.09±0.01	0.08±0.02			
NGM	Zheng	0.20±0.02	0.09±0.01	0.11±0.02			
TE-CDE	Zheng	0.17±0.02	0.09±0.01	0.11±0.01			
CF-ODE	Zheng	0.19±0.03	0.09±0.02	0.11±0.01			
CTP	Zheng	0.18±0.02	0.09±0.01	0.09±0.01			
Linear ODE	MM-25	0.13±0.01	0.04±0.00	0.06±0.02			
Neural ODE	MM-25	0.14±0.02	0.02±0.00	0.05±0.01			
NGM	MM-25	0.15±0.01	0.03±0.01	0.07±0.01			
TE-CDE	MM-25	0.14±0.01	0.02±0.00	0.05±0.01			
CF-ODE	MM-25	0.13±0.01	0.02±0.00	0.04±0.01			
CTP	MM-25	0.13±0.01	0.04±0.01	0.06±0.01			
Linear ODE	MM-50	0.13±0.01	0.03±0.00	0.04±0.00			
Neural ODE	MM-50	0.21±0.01	0.02±0.00	0.06±0.01			
NGM	MM-50	0.15±0.03	0.02±0.01	0.05±0.01			
TE-CDE	MM-50	0.17±0.02	0.03±0.00	0.07±0.02			
CF-ODE	MM-50	0.14±0.02	0.03±0.01	0.05±0.01			
CTP	MM-50	0.19±0.03	0.04±0.01	0.07±0.02			

Table 3: Simulated Data Prediction Performance

4.1.3 ADNI

The Alzheimer’s Disease Neuroimaging Initiative (ADNI) is a multicenter, prospective, naturalistic dataset [49]. The ADNI database consists of a comprehensive collection of neuroimaging, clinical, and genetic data from a large cohort of subjects, including healthy controls, individuals with mild cognitive impairment, and patients with Alzheimer’s disease. We have traversed the ADNI database, excluding mass spectrometry analysis, to match participant demographic information, biomarkers, and family cognitive status data.

We only reserved patients whose available visit record is equal or greater to three to ensure patient data is longitudinal. Features whose missing rate is larger than 30% were discarded. Finally, medical record from 275 patients whose age range from 55 to 90 years old were included. These patients contains 1018 admission records and the average admission time is 3.7. The average interval between two visits is 1.65 years. Each admission record contains 88 features, where 23 features are continuous and 65 features are discrete. The continuous features consists of important bio-markers, e.g., tau protein, amyloid beta protein and cognitive assessment results, e.g., Mini-Mental State Examination (MMSE). Discrete features recorded the usage of medicines.

4.2 Experiment Settings

4.2.1 Baselines

In this study, we used two common seen models and three recently proposed models as baselines.

- Linear ODE. The Linear ODE baseline shares the same structure compared to the CTP, while it use a linear function to model the derivatives of features. The linear ODE does not use ridge loss and DAG loss.
- Neural ODE. Neural ODE shares the same structure compared to the CTP, while it does not use ridge loss and DAG loss to optimize parameters [15].
- NGM. NGM shares the similar structure compared to our CTP, while it only adds group ridge loss to the first layer of neural network to extract causality [50].
- TE-CDE. TE-CDE adopts controlled differential equations to evaluate patient trajectory at any time point and uses a adversarial training approach to adjust unmeasured confounding [21].
- CF-ODE. CF-ODE adopts the Bayesian framework to predict the impact of treatment continuously over time using neural ordinary differential equations equipped with uncertainty estimates [11].

4.2.2 Metrics

- Trajectory Prediction. We used root mean squared error (RMSE) to evaluate the prediction performance on continuous features and the macro average area under the receive operating curve (AUC) to evaluate the prediction performance on discrete features. Of note, the AUC is only applicable in the ADNI dataset as other three datasets only contain continuous features.
- Causal Discovery. We investigate causal discovery performance of the CTP by analyzing the neural connectivity matrix \widehat{D} , where each elements can be mapped to a causal edge. We regard a causal edge is inexistent if its corresponding element is less than a threshold, and vice versa. Then, we use accuracy and F1 to evaluate causal discovery performance. Here, we set threshold to 0.0001. We also use the AUC to evaluate model performance comprehensively. As the element value is not a probability, we use an alternative method to evaluate AUC which calculates the probability that a randomly selected positive subject will have a higher score than a randomly selected negative subject. For baseline models, we followed procedures in their papers to discover causal graphs. We did not investigate causal discovery performance on ADNI dataset for the lack of true causal graph.
- We estimate treatment effect prediction performance via two metrics. First, we use the expectation of the group of CTP models to derive the point estimation of treatment effect. We use the RMSE between the true value and the estimated value to evaluate the performance quantitatively. As the true model maybe unidentifiable, we additional calculate the ratio that whether the true value is included between the lower bound and the upper bound generated by the CTP models.

4.2.3 Treatment Settings

We only evaluate treatment effect on four simulated datasets because it is impossible to access counterfactual result of the ADNI dataset.

- Hao Dataset. We set the neurodegenerative value (i.e., n) to zero at time point 52. Then, we observe the disease progression trajectory under the treatment from 52 to 60.
- Zheng Dataset. We set the neurodegenerative value (i.e., n) to zero at the DPS time 0. Then, we observe the disease progression trajectory under the treatment from 0 to 20.
- MM-25 and MM-50 Dataset. We set the value of the No. 10 node to one at the time point 1. Then, we observe the disease progression trajectory under the treatment from 1 to 10.

Model	Hao Dataset			Zheng Dataset		
	ACC.	F1	AUC	ACC.	F1	AUC
Linear ODE	0.53±0.01	0.60±0.01	0.72±0.01	0.58±0.01	0.64±0.02	0.76±0.03
Neural ODE	0.50±0.02	0.57±0.03	0.54±0.10	0.49±0.01	0.62±0.02	0.43±0.01
NGM	0.54±0.02	0.60±0.02	0.76±0.05	0.59±0.02	0.65±0.02	0.80±0.01
TE-CDE	0.53±0.02	0.59±0.03	0.57±0.10	0.56±0.03	0.65±0.03	0.80±0.02
CF-ODE	0.54±0.02	0.58±0.03	0.55±0.10	0.57±0.01	0.65±0.02	0.80±0.01
CTP	0.56±0.01	0.62±0.02	0.86±0.03	0.61±0.01	0.67±0.01	0.89±0.00
CTP*	1.00	1.00	/	0.88	0.93	/
MM-25 Dataset			MM-50 Dataset			
	ACC.	F1	AUC	ACC.	F1	AUC
Linear ODE	0.75±0.01	0.76±0.01	0.58±0.01	0.87±0.01	0.87±0.01	0.57±0.01
Neural ODE	0.51±0.02	0.67±0.03	0.54±0.10	0.50±0.02	0.66±0.01	0.53±0.02
NGM	0.80±0.02	0.81±0.02	0.68±0.05	0.87±0.02	0.87±0.01	0.58±0.01
TE-CDE	0.80±0.02	0.81±0.02	0.68±0.05	0.87±0.01	0.87±0.01	0.58±0.02
CF-ODE	0.53±0.01	0.56±0.02	0.66±0.03	0.87±0.03	0.87±0.02	0.58±0.02
CTP	0.82±0.01	0.83±0.02	0.74±0.03	0.89±0.01	0.89±0.01	0.63±0.01
CTP*	0.85	0.88	/	0.93	0.92	/

Table 4: Causal Discovery Performance

4.3 Trajectory Prediction

We first investigated the disease progression trajectory prediction performance of the CTP model and baselines. Generally, experimental results showed that our CTP model has good disease progression trajectory prediction ability. It obtained the best performance in the real ADNI dataset, and it obtained comparable performance in the four simulated datasets.

Table 2 describes the prediction performance on the ADNI datasets. Our CTP models generally obtained better performance compared to baselines, as it obtained the first place in combined loss (0.24), combined AUC (0.65), reconstruct RMSE (0.20), reconstructed AUC (0.73), and predict AUC (0.55). The CTP model obtained the second place in predict RMSE (0.29), which is worse than the LODE model (0.26). We did not find significant performance differences in baselines. It is not surprising to found that all models perform better at reconstructing observable trajectories than predicting future trajectories. Meanwhile, we found that predicting future trajectories of discrete variables is difficult. AUCs of all models were less than 0.6, while the L-ODE model only obtained 0.46.

We also conducted trajectory prediction analysis on four simulated datasets (Table 3). We did not report AUC because all simulated datasets only contain continuous variables. The performance of different models varies significantly in different datasets, and there is no model that is significantly better or worse than other models. For example, the L-ODE model obtained significantly worse performance in Hao dataset and Zheng dataset, but it obtained similar or even better performance compared to other models in MM-25 and MM-50 datasets. Our CTP model obtains similar performance compared to NGM, TE-CDE, CF-ODE in Hao dataset, Zheng dataset, and MM-25 dataset, while it obtained worse performance than these baselines in MM-50 dataset.

4.4 Causal Discovery

We also investigated the causal discovery ability of our CTP model and baselines (Table 4). “CTP” indicates the causal discovery performance of a original CTP model, while “CTP*” indicates the causal discovery performance of the CTP model via the causal identification algorithm. It is obvious that the Neural ODE model lack the ability to extract causal relation from features, as its AUC is less than 0.55 in all four datasets. The NGM achieves significantly better causal discovery performance than TE-CDE and CF-ODE, as it is designed for extract causal graphic models from time-series data. Furthermore, our CTP model obtained better performance than the NGM model. The original CTP model obtained 0.86, 0.89, 0.74, 0.63 AUC with respect to the four datasets. We observe original CTP model is easy to identify wrong causal direction. For example, it only obtained 0.56 causal discovery accuracy in Hao dataset. However, its causal discovery performance can be significantly improved if we apply the causal identification algorithm. Specifically, the CTP* model obtained

Model	Hao Dataset			Zheng Dataset		
	Full	Near	Far	Full	Near	Far
Linear ODE	0.77±0.08	0.33±0.05	1.37±0.14	0.79±0.05	0.67±0.02	1.05±0.10
Neural ODE	1.08±0.13	0.54±0.08	1.85±0.19	2.32±0.01	1.39±0.00	4.56±0.02
NGM	0.25±0.01	0.25±0.01	0.26±0.01	0.78±0.04	0.66±0.03	1.00±0.03
TE-CDE	0.32±0.02	0.32±0.01	0.31±0.01	4.88±0.01	1.75±0.01	9.21±0.01
CF-ODE	0.57±0.03	0.38±0.02	0.84±0.05	0.36±0.03	0.24±0.02	0.55±0.06
CTP	0.16±0.01	0.16±0.00	0.16±0.01	0.32±0.03	0.26±0.02	0.47±0.03

	MM-25 Dataset			MM-50 Dataset		
	Full	Near	Far	Full	Near	Far
Linear ODE	1.13±0.05	1.11±0.07	1.22±0.04	1.51±0.01	1.52±0.00	1.51±0.01
Neural ODE	1.25±0.04	1.23±0.05	1.60±0.03	1.48±0.03	1.43±0.03	1.67±0.02
NGM	0.89±0.03	0.91±0.04	0.79±0.02	2.41±0.08	2.24±0.05	3.12±0.13
TE-CDE	1.25±0.09	1.19±0.11	1.52±0.15	1.50±0.04	1.45±0.05	1.70±0.08
CF-ODE	1.29±0.04	1.22±0.03	1.59±0.05	1.64±0.09	1.58±0.07	1.88±0.13
CTP	0.78±0.03	0.74±0.05	0.88±0.07	1.20±0.06	1.15±0.08	1.43±0.05

Table 5: Treatment Effect Estimation

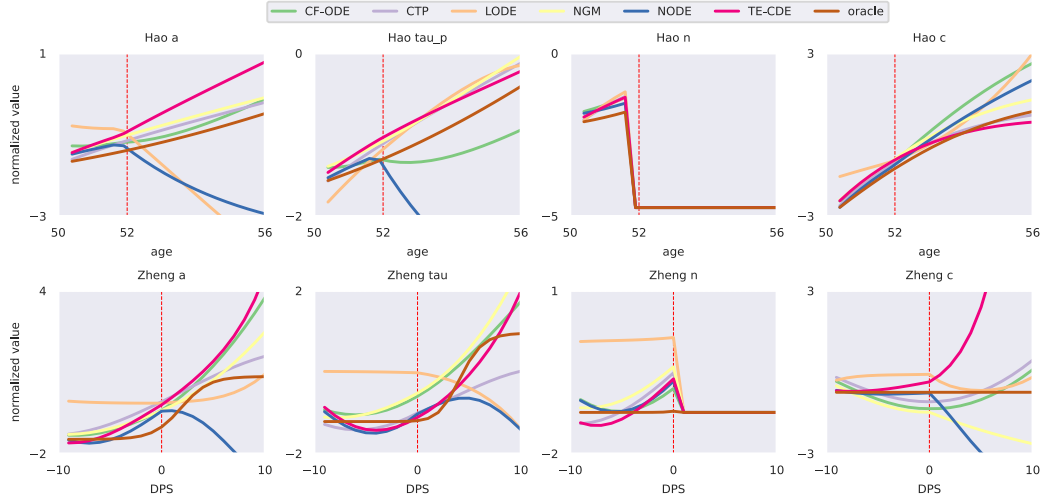


Figure 4: Treatment Effect Prediction

0.44, 0.27, 0.07, 0.04 performance gain in accuracy with respect to four datasets and 0.38, 0.26, 0.05, 0.03 performance gain in F1. We can summarize that our original CTP model can identify causal relation between features better than all baselines, and its performance can be further improved by utilizing the causal identification algorithm.

4.5 Treatment Effect Analysis

Table 5 describes the performance of predicting the effect of a given treatment of the CTP model and baselines in four datasets. The “Full” column indicates the general difference between predicted trajectories and oracle trajectories of features. The “Near” column indicates the differences in the first half trajectories and the “Far” column indicates the second half. The CTP model obtained significantly better performance than all baselines. For example, The full RMSE of Neural ODE in Hao dataset is 1.08, about six times more than the CTP model (0.16). The NGM model obtained best performance among baselines, while the CTP model decreases about 40% differences in RMSE. The performance of our CTP model is also significantly better in MM-25 and MM-50 datasets, though the performance gain is not as significant as it in Hao dataset and Zheng dataset. Our CTP model is more appropriate to be used to evaluate the treatment effect to dynamical system with dozens of variables.

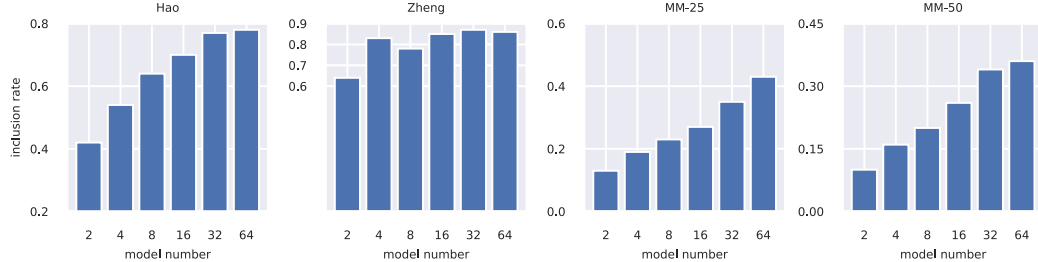


Figure 5: Treatment Inclusion

We also qualitatively analyzed why our CTP model obtained significantly better performance than baselines in Figure 4. For the space limit, we only draw feature trajectories of Hao model and Zheng model. The figure shows that some trajectories generated by baselines changed unexpectedly after the treatment. For example, the predicted trajectory of a in Hao dataset of Linear ODE, Neural ODE decrease rapidly after we apply the treatment, while the treatment actually does not affect the trajectory of a . Similar deviations also occurs in other figures. For example, Neural ODE, CF-ODE in τ_p in Hao dataset, Neural ODE in a in Zheng dataset, Linear ODE in τ in Zheng dataset, NGM and TE-CDE in c in Zheng dataset. These models cannot predict feature trajectories under a treatment well mainly because they utilized correlational information between features. Our CTP model overcome this limitation because it utilize causal information between features to conduct analysis.

We finally investigated the effectiveness of the estimated bound. We evaluate the bound quality by estimating whether a true feature value is included in the bound. We calculated the rate of inclusion in Figure 5. We found that the inclusion rate is relevant to the number of CTP models. The more the more, the better the performance. For example, the inclusion rate of Hao dataset is 0.22 when we only use two models, while it gradually increases to 0.71 when we applied 64 models. Inclusion rate on other datasets also shows similar tendency. Therefore, we argue that our method is able to estimate the possible influence of a treatment in a relatively long time span, which will assist better clinical decision. It is worth to note that different dataset requires different number of parallel models. The inclusion rate converges when model number is larger than 32 in Hao dataset, while it converges when model number is larger than eight in Zheng dataset. The inclusion rate of MM-25 dataset and MM-50 dataset is significantly lower than the other two dataset. It may be attributed to our model mistakenly estimate some causal directions for some features and our model cannot generate appropriate bound for them.

5 Discussion

Prognostic analysis aims to assist clinical decision-making and improve prognosis. In the past, we often transformed this goal into developing accurate prognostic models. For diseases with clear treatment strategies, this is indeed the case. For example, for patients with coronary heart disease, high-risk patients should undergo PCI as much as possible. As long as we can accurately identify high-risk patients, we can issue targeted interventions to reduce their risks. However, for chronic diseases like Alzheimer’s disease or heart failure, this is insufficient. Due to patient heterogeneity, different patients with poor prognosis will have different suitable treatment plans. Knowing only about poor prognosis is not enough to let us know which treatment method is suitable for them. Therefore, accurate predictions do not necessarily mean they can assist clinical decision-making. For complex chronic diseases, when designing prognostic models, we actually hope that the prognostic models can answer counterfactual queries, that is, the model is still accurate in predicting the prognosis of data after artificial manipulation. If the model can accurately predict the subsequent impact of an intervention, it can naturally assist doctors in making more effective decisions. However, current models based on deep learning are trained based on observational data and find it hard to answer ‘what if’ questions. Our experiments have also proved this. All baseline models met trajectory deviation problem when we apply a treatment. For general deep learning models, even though they can achieve extremely accurate predictive performance, once we manually manipulate the data input, their predictive ability will plummet drastically, becoming completely unusable. Therefore,

in this paper, we attempted to use observational data to train a prognostic model that can answer counterfactual queries.

Uncovering the causal relationship hidden in the data is the core of answering counterfactual queries. Only after understanding the causal structure between data, can we correctly adjust backdoor variables and avoid the problem of reversing cause and effect. In this study, we combined score-based methods with NODE methods to propose an effective causal mining method that can be applied to sequence data. This method can complete the mining of causal structure and patient prediction in an end-to-end manner. At the same time, considering the instability of causal discovery algorithms, we also proposed a causal judgment algorithm to stably reveal the causal relationship from the data. Our experimental results on two simulated Alzheimer’s disease datasets and two random datasets show that the method proposed in this study can effectively mine causal relationships for physiological processes that are not causally related, and its performance is better than previous methods based on sparse penalty and Granger causal mining. At the same time, we also compared this model with the Latent NODE model. The comparison results show that while our model has achieved causal discovery capabilities, it has not led to a significant decline in the model’s predictive performance for the prognosis trajectory in the five experimental datasets. Our CTP model has achieved near SOTA performance.

After uncovering the causal relationships, we conducted an intervention effect analysis study. It is worth noting that existing research shows that when there are hidden variables in the data, the model may be unidentifiable. In theory, there could be an infinite number of models, all of which could generate the observed dataset. Therefore, in this study, we filled the possible parameter space of the model by training a group of models with consistent causal structures but as different parameters as possible. We used the range covered by this group of models as an estimate of the intervention effect to plot the possible range of the patient’s future evolution trajectory. Qualitative experimental results show that the estimated range of the model contains the true value of the disease evolution trajectory after intervention. At the same time, we also conducted an intervention effect analysis using the average trajectory predicted by the model. The related results show that our model can more accurately predict the overall disease evolution trajectory of the patient after the intervention, and its performance is superior to the existing baseline model.

This study has two advantages and two shortcomings. The first advantage is that we have fully evaluated the model’s performance in causal discovery, trajectory prediction, and quantitatively and qualitatively evaluated the model’s performance in intervention effect analysis. It comprehensively explains that our model can be used for prognostic prediction and intervention effect analysis of long-term disease evolution trajectories. Previous studies usually do not focus on predicting an entire trajectory, but only on the prognosis at a single isolated time point. And previous research generally deals with causal discovery and intervention effect analysis separately, with few studies completing a full inference of causal discovery and intervention effect analysis. The second advantage is that we conducted comprehensive experiments. In this study, we chose a real public clinical dataset, two simulated Alzheimer’s disease amyloid deposition datasets, and two completely simulated high-dimensional datasets for analysis. At the same time, we chose five related models published in recent years as baselines, fully proving the superior performance and universality of the CTP model. This study also has two shortcomings. The first shortcoming is that we assumed that the causal structure of the data constitutes a directed acyclic graph, which means that our model cannot handle feedback phenomena in dynamic time series systems. The second shortcoming is that we only conducted complete experiments on simulated datasets. We only conducted predictive analysis of prognosis trajectories on real datasets. In future research, we will try to evaluate the performance of model results in causal analysis on real datasets.

6 Conclusion

This study introduces the causal progression analysis (CPA) framework, which addresses the challenges of conducting treatment analysis in the presence of both unmeasured confounders and a need for causal interpretability. The framework combines trajectory prediction and causal graph discovery to estimate initial values and change rates of features, allowing for the prediction of disease progression trajectories. By incorporating a causal graph into the dynamic system, the framework ensures that each feature is predicted only by itself and its causal ancestors. Furthermore, the framework tackles the issue of unmeasured confounders by identifying correlated errors and constraining the

possible effect space of confounders using observed data. Experimental results demonstrate that the CPA framework performs comparably or better than baselines in discovering causal relationships, predicting disease progression trajectories. Overall, this framework offers a novel approach to support clinical decision-making.

References

- [1] Tahami Monfared, A. A., M. J. Byrnes, L. A. White, et al. Alzheimer’s disease: epidemiology and clinical progression. *Neurology and therapy*, 11(2):553–569, 2022.
- [2] Gill, T. M. The central role of prognosis in clinical decision making. *JAMA*, 307(2):199–200, 2012.
- [3] Wang, C., Y. Li, Y. Tsuboshita, et al. A high-generalizability machine learning framework for predicting the progression of alzheimer’s disease using limited data. *NPJ digital medicine*, 5(1):43, 2022.
- [4] Severson, K. A., L. M. Chahine, L. A. Smolensky, et al. Discovery of parkinson’s disease states and disease progression modelling: a longitudinal data study using machine learning. *The Lancet Digital Health*, 3(9):e555–e564, 2021.
- [5] Saboo, K., A. Choudhary, Y. Cao, et al. Reinforcement learning based disease progression model for alzheimer’s disease. In *Advances in Neural Information Processing Systems*, vol. 34, pages 20903–20915. 2021.
- [6] Wilkinson, J., K. F. Arnold, E. J. Murray, et al. Time to reality check the promises of machine learning-powered precision medicine. *The Lancet Digital Health*, 2(12):e677–e680, 2020.
- [7] Moraaffah, R., M. Karami, R. Guo, et al. Causal interpretability for machine learning-problems, methods and evaluation. *ACM SIGKDD Explorations Newsletter*, 22(1):18–33, 2020.
- [8] Yao, L., Z. Chu, S. Li, et al. A survey on causal inference. *ACM Transactions on Knowledge Discovery from Data (TKDD)*, 15(5):1–46, 2021.
- [9] Neal, B. *Introduction to Causal Inference*. 2020.
- [10] Balazadeh Meresht, V., V. Syrgkanis, R. G. Krishnan. Partial identification of treatment effects with implicit generative models. *Advances in Neural Information Processing Systems*, 35:22816–22829, 2022.
- [11] De Brouwer, E., J. Gonzalez, S. Hyland. Predicting the impact of treatments over time with uncertainty aware neural differential equations. In *International Conference on Artificial Intelligence and Statistics*, pages 4705–4722. 2022.
- [12] Gunsilius, F. A path-sampling method to partially identify causal effects in instrumental variable models. *arXiv preprint arXiv:1910.09502*, 2019.
- [13] Gunsilius, F. F. Nontestability of instrument validity under continuous treatments. *Biometrika*, 108(4):989–995, 2021.
- [14] Stanhope, S., J. E. Rubin, D. Swigon. Identifiability of linear and linear-in-parameters dynamical systems from a single trajectory. *SIAM Journal on Applied Dynamical Systems*, 13(4):1792–1815, 2014.
- [15] Chen, R. T., Y. Rubanova, J. Bettencourt, et al. Neural ordinary differential equations. In *Advances in neural information processing systems*, vol. 31. 2018.
- [16] Lachapelle, S., P. Brouillard, T. Deleu, et al. Gradient-based neural dag learning. In *International Conference on Learning Representations*. 2020.
- [17] Brunton, S. L., J. L. Proctor, J. N. Kutz. Discovering governing equations from data by sparse identification of nonlinear dynamical systems. *Proceedings of the national academy of sciences*, 113(15):3932–3937, 2016.
- [18] Chen, Z., Y. Liu, H. Sun. Physics-informed learning of governing equations from scarce data. *Nature communications*, 12(1):6136, 2021.
- [19] Alaa, A. M., M. van der Schaar. Attentive state-space modeling of disease progression. In *Advances in neural information processing systems*, vol. 32. 2019.

[20] Lim, B., M. van der Schaar. Disease-atlas: Navigating disease trajectories using deep learning. In *Machine Learning for Healthcare Conference*, pages 137–160. 2018.

[21] Seedat, N., F. Imrie, A. Bellot, et al. Continuous-time modeling of counterfactual outcomes using neural controlled differential equations. *International Conference on Machine Learning*, 2022.

[22] Alaa, A., E. Mayer, M. Barahona. Ice-node: Integration of clinical embeddings with neural ordinary differential equations. In *Proceedings of Machine Learning Research*. 2022.

[23] Duan, H., Z. Sun, W. Dong, et al. On clinical event prediction in patient treatment trajectory using longitudinal electronic health records. *IEEE Journal of Biomedical and Health Informatics*, 24(7):2053–2063, 2019.

[24] Tan, Q., M. Ye, B. Yang, et al. Data-gru: Dual-attention time-aware gated recurrent unit for irregular multivariate time series. In *Proceedings of the AAAI Conference on Artificial Intelligence*, vol. 34, pages 930–937. 2020.

[25] Tipirneni, S., C. K. Reddy. Self-supervised transformer for sparse and irregularly sampled multivariate clinical time-series. *ACM Transactions on Knowledge Discovery from Data (TKDD)*, 16(6):1–17, 2022.

[26] Wang, Y., W. Huang, M. Gong, et al. Identifiability and asymptotics in learning homogeneous linear ode systems from discrete observations. *arXiv preprint arXiv:2210.05955*, 2022.

[27] Cheng, Y., R. Yang, T. Xiao, et al. Cuts: Neural causal discovery from irregular time-series data. In *International Conference on Learning Representations*. 2023.

[28] Amornbunchornvej, C., E. Zheleva, T. Berger-Wolf. Variable-lag granger causality and transfer entropy for time series analysis. *ACM Transactions on Knowledge Discovery from Data*, 15(4):1–30, 2021.

[29] Bica, I., A. Alaa, M. Van Der Schaar. Time series deconfounder: Estimating treatment effects over time in the presence of hidden confounders. In *International Conference on Machine Learning*, pages 884–895. 2020.

[30] Ma, J., R. Guo, C. Chen, et al. Deconfounding with networked observational data in a dynamic environment. In *Proceedings of the 14th ACM International Conference on Web Search and Data Mining*, pages 166–174. 2021.

[31] Cao, D., J. Enouen, Y. Wang, et al. Estimating treatment effects from irregular time series observations with hidden confounders. In *AAAI Conference on Artificial Intelligence*. 2023.

[32] Ashman, M., C. Ma, A. Hilmkil, et al. Causal reasoning in the presence of latent confounders via neural admg learning. *International Conference on Learning Representations*, 2023.

[33] Wang, Z., S. Shen, Z. Wang, et al. Unbiased sequential recommendation with latent confounders. In *Proceedings of the ACM Web Conference 2022*, pages 2195–2204. 2022.

[34] Bhattacharya, R., T. Nagarajan, D. Malinsky, et al. Differentiable causal discovery under unmeasured confounding. In *International Conference on Artificial Intelligence and Statistics*, pages 2314–2322. 2021.

[35] Löwe, S., D. Madras, R. Zemel, et al. Amortized causal discovery: Learning to infer causal graphs from time-series data. In *Conference on Causal Learning and Reasoning*, pages 509–525. 2022.

[36] Kingma, D. P., M. Welling. Auto-encoding variational bayes. In *International Conference on Learning Representations*. 2014.

[37] Jang, E., S. Gu, B. Poole. Categorical reparameterization with gumbel-softmax. *International Conference on Learning Representations*, 2017.

[38] Blaser, N., L. S. Vizcaya, J. Estill, et al. Gems: an r package for simulating from disease progression models. *Journal of Statistical Software*, 64(10):1, 2015.

[39] Suttorp, M. M., B. Siegerink, K. J. Jager, et al. Graphical presentation of confounding in directed acyclic graphs. *Nephrology Dialysis Transplantation*, 30(9):1418–1423, 2015.

[40] Hao, W., S. Lenhart, J. R. Petrella. Optimal anti-amyloid-beta therapy for alzheimer’s disease via a personalized mathematical model. *PLoS computational biology*, 18(9):e1010481, 2022.

- [41] Zheng, X., B. Aragam, P. K. Ravikumar, et al. Dags with no tears: Continuous optimization for structure learning. In *Advances in Neural Information Processing Systems*, vol. 31. 2018.
- [42] Rodriguez, I. D. J., A. Ames, Y. Yue. Lyanet: A lyapunov framework for training neural odes. In *International Conference on Machine Learning*, pages 18687–18703. PMLR, 2022.
- [43] Miao, H., X. Xia, A. S. Perelson, et al. On identifiability of nonlinear ode models and applications in viral dynamics. *SIAM review*, 53(1):3–39, 2011.
- [44] Kostrikov, I., O. Nachum, J. Tompson. Imitation learning via off-policy distribution matching. In *International Conference on Learning Representations*. 2020.
- [45] Zheng, H., J. R. Petrella, P. M. Doraiswamy, et al. Data-driven causal model discovery and personalized prediction in alzheimer’s disease. *npj Digital Medicine*, 5(1):137, 2022.
- [46] Mielke, M. M., C. E. Hagen, A. M. Wennberg, et al. Association of plasma total tau level with cognitive decline and risk of mild cognitive impairment or dementia in the mayo clinic study on aging. *JAMA neurology*, 74(9):1073–1080, 2017.
- [47] Virtanen, P., R. Gommers, T. E. Oliphant, et al. Scipy 1.0: fundamental algorithms for scientific computing in python. *Nature methods*, 17(3):261–272, 2020.
- [48] Zhang, Y., Y. Guo, Z. Zhang, et al. Universal framework for reconstructing complex networks and node dynamics from discrete or continuous dynamics data. *Physical Review E*, 106(3):034315, 2022.
- [49] Petersen, R. C., P. S. Aisen, L. A. Beckett, et al. Alzheimer’s disease neuroimaging initiative (adni): clinical characterization. *Neurology*, 74(3):201–209, 2010.
- [50] Bellot, A., K. Branson, M. van der Schaar. Neural graphical modelling in continuous-time: consistency guarantees and algorithms. 2022.